Adiabatic Equilibrium Calculations of Major Radius Compression in a Tokamak

D.B.Albert, H.Winter

IPP III/58 February 198o

MAX-PLANCK-INSTITUT FÜR PLASMAPHYSIK

8046 GARCHING BEI MÜNCHEN

MAX-PLANCK-INSTITUT FÜR PLASMAPHYSIK

GARCHING BEI MÜNCHEN

Adiabatic Equilibrium Calculations of Major Radius Compression in a Tokamak

D.B.Albert, H.Winter

IPP III/58 February 198o

Die nachstehende Arbeit wurde im Rahmen des Vertrages zwischen dem Max-Planck-Institut für Plasmaphysik und der Europäischen Atomgemeinschaft über die Zusammenarbeit auf dem Gebiete der Plasmaphysik durchgeführt.

Abstract

Equilibrium calculations which conserve adiabatic quantities (magnetic fluxes, particle number and entropy) during major-radius compression in a tokamak have been made using a flux surface averaged description of the plasma behaviour in order to solve the two-dimensional plasma equilibrium equation. Boundary conditions are chosen to avoid skin current formation during compression and the changes of the ohmic heating flux required to maintain this condition are determined. Comparisons are made between the plasma parameter variations determined from these computations and the scaling behaviour predicted by a large aspect ratio approximation to the adiabatic constraints.

1. Introduction

The concept of adiabatic compression of a tokamak discharge can, in principle, provide a highly efficient method for auxiliary heating of a plasma.Present scaling laws for the confinement time τ_E, however, indicate that major radius compression of an ohmically heated plasma gives no large improvement in the achievable temperatures over ohmic heating alone at the compressed plasma position /1/. The main advantage of this form of compression is realized when it is used to multiply the heating effect of neutral beam or RF heating of the pre-compression plasma as demonstrated in experiments in ATC /2/. Such a method may be used to attain an ignited state by compressing a plasma,whose opacity (density-minor radius product) is determined by neutral beam penetration into the plasma, until the $\bar{n}a$ factor reaches the value required for ignition /3/. If an ignited plasma is achieved in this manner, the compression techniques may also be used for thermal stability control of the burning plasma by regulating the temperature with alternating compression and decompression steps /4/.

Approximate scaling laws for the behaviour of averaged parameters of a plasma subjected to adiabatic compression may be determined by applying the conditions of flux and entropy conservation to a simple cylindrical model of the plasma /5/. In the design of an experiment which uses adiabatic compression to achieve ignition, however, a more detailed description of the behaviour is required to take into account finite ß and higher order toroidal effects as well as variations of parameters over the plasma cross-section. This information may be obtained from calculations of toroidal plasma equilibria which conserve adiabatic quantities. By performing such calculations with a free plasma boundary, it is also possible to describe the manner in which the plasma shape adjusts to changes in the external fields which produce the compression. A description of the toroidal field behaviour

which provides a good approximation to the experimental conditions may also be employed in these calculations by using boundary conditions which correspond to a constant current in the toroidal field coils. Because the total flux linked by the plasma may be adjusted by varying the flux of the ohmic heating coils, the programming of the poloidal field which is necessary to suppress skin current formation during compression may also be determined using this technique.

This paper presents a description of the basic concepts of a flux-conserving adiabatic equilibrium calculation (Sec.2) together with some details of the computational methods employed including assessments of its accuracy (Sec.3). Results of these computations for the case of major radius compression in a general case (Sec.4) are presented as well as calculations of the compression phase in the ZEPHYR compact ignition experiment design (Sec.5).

2. Equilibrium Calculations under Adiabatic Conditions

The assumption of adiabatic behaviour during compression implies that losses must be negligible on the time scale of the changes in the external field producing the compression. Calculations simulating compression experiments on ATC /6,7/ for example, have indicated that radiation losses due to small amounts of heavy metal impurities can, under some conditions, have a significant effect on the scaling of plasma parameters. In order for the adiabaticity approximation to be valid, we require that the compression time scale be short compared with the resistive skin time as well as the particle and energy confinement times. The first condition for the classical skin time is easily satisfied in a plasma which is to be compressed to ignition. For the second and third constraints, which could be more difficult to fulfil, losses may be compensated by additional heating and refuelling during the early compression phase. During the later stage of compression, when neutral beam penetration would be considerably reduced, the fusion energy output will have increased so that, in the neighbourhood of the ignition point, the deviation from adiabaticity will be small. This situation will also occur in the case of burn stabilization by compression/decompression techniques.

The equilibrium of a toroidal plasma may be described in terms of a poloidal flux function ψ, defined by the relation

$$\underset{\sim}{B} = f\underset{\sim}{\nabla}\phi + \underset{\sim}{\nabla}\phi \times \underset{\sim}{\nabla}\psi$$

where ϕ is the toroidal angle and $f=RB_\phi$ is the flux function of poloidal currents /11/. Using this relation in the equation for plasma equilibrium $\underset{\sim}{J} \times \underset{\sim}{B} = \underset{\sim}{\nabla} P$, we obtain the Grad-Shafranov equation

$$\Delta^*\psi = R^2\nabla\cdot\left(\frac{1}{R^2}\nabla\psi\right) = -\mu_o R^2 \frac{\partial P}{\partial \psi} - f\frac{\partial f}{\partial \psi} \qquad (2)$$

where the total pressure $P(\psi)$, and $f(\psi)$ are functions of ψ. (R is the major radial distance from the axis of toroidal symmetry; see Fig.1). In the absence of losses, the poloidal flux ψ, and the toroidal flux $\chi = \int q\, d\psi$ (where q is the safety factor), within the plasma will be conserved. From these conservation conditions, it follows that q is also conserved and can thus be treated as a function of ψ.

Defining the quantity $V(\psi)$, as the volume within as surface of constant ψ so that

$$\frac{\partial V}{\partial \psi} = 2\pi \oint_{\psi} \frac{R\,dl}{|\nabla \psi|} \quad \text{and} \quad V = \oint \frac{R^2}{|\nabla \psi|} \frac{\partial \psi}{\partial R}\, dl,$$

it may be deduced from the condition of entropy conservation that the quantity

$$\mu(\psi) = p(\psi) \left(\frac{dV}{d\psi}\right)^{\gamma} \qquad (3)$$

is also conserved ($p=\mu_o P$ and $\gamma = 5/3$ is the adiabatic constant).

In order to solve the equilibrium equation (2) while conserving the adiabatic functions $q(\psi)$ and $\mu(\psi)$, we have used the technique introduced by Grad /8/ of solving a flux-surface averaged form of the equilibrium condition. For this purpose, we define the average of a quantity over a surface of constant ψ as

$$\langle X \rangle_{\psi} = \frac{\int \frac{X}{|\nabla \psi|}\, ds}{\int \frac{ds}{|\nabla \psi|}}$$

and it may then be shown that $\left\langle \frac{\Delta^* \psi}{R^2} \right\rangle_{\psi} = (K \psi')'$

where $K = \left\langle \left| \frac{\nabla V}{R} \right|^2 \right\rangle_{\psi}$ and $'$ denotes differentiation with respect to V. Because $p(\psi)$ and $f(\psi)$ are constant over a flux surface, we may then derive the constraint

$$(K \psi')' = -\dot{p} - A f \dot{f} \qquad (4)$$

with $A = \left\langle \frac{1}{R^2} \right\rangle_{\psi}$. This is a first-order differential equation in

$\psi(V)$ which can be solved subject to given functions $q(\psi)$ and $\mu(\psi)$ by using eq.(3) for $p(\psi)$ and the relation

$$f(\psi) = \frac{4\pi 2 \psi'}{A} q(\psi) \qquad (5)$$

Flux conserving calculations of this form have been made previously in order to study ß limits in the flux-conserving tokamak concept /9/ as well as neutral beam heating of an adiabatic plasma /10/. In these calculations, which did not allow complete freedom of the plasma boundary, it was observed that the poloidal current function f, at the plasma boundary increased above the vacuum value. To make this behaviour consistent with the toroidal field in the vacuum would require either an increase in the current in the toroidal field coils or a poloidal skin current at the boundary. For an experimentally realistic situation, the value of f_o, which is determined exclusively by the toroidal field coil current, will remain essentially constant and the continuity of f across the plasma boundary will be maintained by a change in the plasma boundary /10/.

In the general case, when a plasma is heated or compressed on a time scale fast enough to justify the flux conservation assumption, surface currents will be produced. If the plasma pressure vanishes at the plasma boundary, such surface currents must appear simultaneously both in poloidal and toroidal directions in order to satisfy the force balance. A rapid change in the OH flux for example will induce toroidal surface currents which would give rise to a small compression or decompression of the toroidal field and thus a discontinuity in f corresponding to a poloidal surface current. Although the exact consequences of such surface currents are not completely clear, one would expect an increase in MHD instability due to the presence of a double tearing layer produced by a toroidal skin current and possibly a corresponding deterioration of the plasma confinement.

Because the current density distribution within the plasma is determined essentially by the $q(\psi)$ conservation, the requirement for conservation of flux within the plasma is usually met by the appearance of a poloidal skin current which does not affect the q-profile within the plasma but adjusts the total flux linked by the plasma surface. If the flux of the OH system is programmed to make this adjustment then these skin currents can be avoided. For fixed initial plasma parameters, such programming could be effected by appropriately designing the spatial distribution of the vertical field system, but this method would allow no flexibility to adjust for different parameters. As it is, in fact, very difficult to design a free boundary equilibrium code which could adequately handle both volume and surface currents in the plasma simultaneously, we determine at each iteration of the equilibrium calculation, consistent with the changes of the plasma parameters, the change of the OH flux necessary to maintain flux conservation so that

$$\psi_{tot} = \psi_{pl} + \psi_{ext} + \psi_{OH}$$

where ψ_{pl} is the plasma flux, ψ_{ext} the flux due to the vertical field coils and ψ_{OH} is the change in the flux of the ohmic heating coil system necessary to avoid skin current formation during the compression. A more detailed discussion of surface currents and other inductive effects in flux-conserving tokamaks is given in reference /13/.

3. Description of Computational Algorithm

Calculation of the evolution of plasma equilibria during adiabatic compression begins with the determination of an equilibrium corresponding to the uncompressed state for which, in the cases presented here, a current density distribution of the following form is used

$$j(\psi) = \mu_o (\alpha_1 \psi_d + \alpha_2 \psi_d^2) R + \frac{(\alpha_3 \psi_d + \alpha_4 \psi_d^2)}{R} \quad (6)$$

where $\psi_d = \psi - \psi_c$; ψ_c is the flux at the plasma boundary. With this function, the α parameters can be adjusted to produce a desired total plasma current and β_p, since if $\frac{\alpha_2}{\alpha_1} = \frac{\alpha_4}{\alpha_3}$,

then $\beta_p \approx \frac{1}{1 + \frac{\alpha_3}{\alpha_1 R_o^2}}$, where R_o is the radius of the magnetic axis. Since the above functional form for the current density specifies $\frac{\partial p}{\partial \psi}$ and $\frac{f \partial f}{\partial \psi}$, we may independently choose f_o corresponding to a specific value of the vacuum toroidal magnetic field.

For the solution of the 2-dimensional equilibrium eq.(2) in an infinite domain, we have employed the direct Poisson solver technique of von Hagenow and Lackner /11,12/. In the initial equilibrium determination, ψ_{pl} is calculated by iterating with the solution of the equation

$$\Delta^* \psi_{pl}^{N+1} = - R\, j\, (\psi_{tot}^{N})$$

from which $\psi_{tot}^{N+1} = \psi_{pl}^{N+1} + \psi_{ext}$ is computed by choosing ψ_{ext} corresponding to the desired plasma position.

For the flux-conserving calculation, the geometrical quantities K and A are determined using flux contours obtained from the equilibrium solution by quadratic interpolation between the

points of the two dimensional grid and then evaluating the integrals

$$K = 2\pi \dot{V} \oint \frac{|\nabla\psi|}{R}\, dl \quad \text{and} \quad A = \frac{2\pi}{\dot{V}} \oint \frac{dl}{R\nabla\psi} \qquad (7)$$

$$\text{with} \quad \dot{V} = \frac{\partial V}{\partial \psi}$$

This information may then be used in the solution of the averaged equilibrium eq.(4) which can best be done by eliminating ψ' in the following manner.

Defining $\nu = \frac{1}{4\pi^2 q}$ and $\alpha = fA$,

we have from eq.(5) that $\psi' = \alpha\nu$
and thus $p = \mu(\alpha\nu)^\gamma$. Making these substitutions into eq.(4) it may be shown that /14/

$$f\dot{f} = -f^2 \frac{\left[\nu \frac{d}{d\psi}(AK\nu) + \alpha^{\gamma-2} A^{1-\gamma} \frac{d}{d\psi}(\mu A^\gamma \nu^\gamma)\right]}{1 + A(K\nu^2 + \gamma\mu\nu^\gamma\alpha^{\gamma-2})} \qquad (8)$$

$$\text{and} \quad \dot{p} = \frac{\alpha^\gamma \left[(1+AK\nu^2)A^{-\gamma}\frac{d}{d\psi}(\mu A^\gamma \nu^\gamma) - \mu\gamma\nu^{\gamma+1}\frac{d}{d\psi}(AK\nu)\right]}{1 + A(K\nu^2 + \gamma\mu\nu^\gamma\alpha^{\gamma-2})} \qquad (9)$$

where $\dot{}$ denotes differentiation with respect to ψ .

From eq.(8), we can derive an integral equation for f which may be solved by Picard iteration

$$\frac{f\dot{f}}{f^2} = \frac{\dot{f}}{f} = \frac{d}{d\psi}(\ell n\, f) = F(\psi)$$

$$\text{so} \quad f = f_o \exp\left(-\int_\psi^{\psi_c} F(\psi)\, d\psi\right)$$

$$\text{and thus} \quad f = f_o \exp\left(\int_\psi^{\psi_c} \frac{\frac{d}{d\psi}(AK\nu)\nu + \alpha^{\gamma-2}A^{1-\gamma}\frac{d}{d\psi}(\mu A^\gamma \nu^\gamma)d\psi}{1 + A(K\nu^2 + \gamma\mu\nu^\gamma\alpha^{\gamma-2})}\right) \qquad (10)$$

Using this result, it is possible to determine the volume within a flux surface $V(\psi)$, from $\frac{dV}{d\psi} = \frac{1}{\nu f A}$

$$\text{so } V(\psi) = \int_{\psi_o}^{\psi} \frac{1}{\nu f A}\, d\psi \qquad (11)$$

This calculation must be used in the evaluation of the integral in eq.(10) because K and A, being geometrical quantities, are functions of the volume associated with a particular ψ value.

With these relations as the basic components of the solution, the algorithm for obtaining an equilibrium which conserves adiabatic quantities in the compressed state consists of the following steps (step numbers refer to the flow chart in Fig.2).

Step 1: From the p and f functions of the equilibrium in the uncompressed state, compute $q(\psi)$ and $\mu(\psi)$ using the relations given by eq.(3) and (5). Determine ψ_{ext} due to the increased vertical field producing the compression. Find ψ_o and ψ_c, the values of the total flux at the magnetic axis and the plasma boundary respectively.

Step 2: Flux Conserving step: Calculate $\psi_{tot} = \psi_{pl} + \psi_{ext}$ and also the value of ψ_{tot} at the magnetic axis ψ_{mag}. Recompute ψ_{tot} as $\psi_{pl} + \psi_{OH}$ where $\psi_{OH} = \psi_o - \psi_{mag}$ thereby ensuring that the flux at the magnetic axis is always ψ_o.

Step 3: Determine contours of ψ_{tot} as well as values of the contour integrals V_j, ψ_j, K(Vj) and A(Vj) for flux values ψ_j at equally spaced intervals between ψ_o and ψ_c.

Step 4: Solve the flux-surface averaged equilibrium equation in the form given by eq.(10) which maintains $f(\psi) = f_o$ at the plasma boundary. The evaluation of this integral is done iteratively in the following steps:

a) Find K and A values at volumes corresponding to Ψ_j values. This is done by cubic spline interpolation of the K(V) and A(V) values obtained from the contour integrals performed in step 3.

b) Calculate Ψ derivatives in the integrand of eq.(10) by differentiating a cubic spline fit to the points.

c) Determine $f^{N+1}(\Psi)$ by evaluating the integral in eq.(10) using $\alpha = f^N(\Psi)A$ from the previous iteration. Also compute $f\dot{f}(\Psi_j)$ from eq.(8) and compare with the results of the previous iteration. If converged, determine $\dot{p}(\Psi_j)$ from eq. (9) thus completing the inner loop.

d) Compute the volumes $V(\Psi_j)$ using the integral in eq.(11) and return to step a).

Step 5: Test convergence of the outer iteration by calculating the q values from $q = \frac{fA}{4\pi^2\Psi'}$, with the A and Ψ' values from the contour integrals and the f values determined in step 4 and compare with the desired $q(\Psi_j)$ values.

Step 6: For each point of the 2-dimensional grid, a new value for Ψ is found by interpolating the $\Psi(V)$ function obtained in step 4 at the volume value determined by the contour integral. In this way, the information derived from the solution of the flux-surface averaged equation is transferred to the 2-D problem with the geometry of the flux surfaces held fixed.

Step 7: New values for the right hand side of eq.(2) are then obtained by interpolating the $\dot{p}$ and $f\dot{f}$ functions found in step 4 at the Ψ values determined in step 6. Eq.(2) is then solved to find Ψ_p for the next iteration which begins again at step 2.

This technique of using the solution of the flux-surface averaged equilibrium constraint to determine the right-hand side of the 2-dimensional equation thus results in an equilibrium state

which conforms to the specified $q(\psi)$ and $\mu(\psi)$ functions with the free boundary adjusted to maintain the continuity of $f(\psi)$. Because it begins with an independently determined equilibrium, this algorithm may be tested and its accuracy assessed by performing the calculation without changing ψ_{ext} from the uncompressed value. For this case, an accuracy of 3×10^{-3} in the calculated q values was typically obtained while the flux values were found to be conserved to within 10^{-3} of the maximum flux, ψ_o.

In applying this algorithm to the determination of plasma equilibria during adiabatic compression, it was generally observed that values of q determined in step 5 of the algorithm would converge to less than 4×10^{-3} of the desired values within 25 iterations of the outer loop (see Fig.3) for a 15 % increase in the magnitude of ψ_{ext}. The inner iteration loop which solves the averaged equilibrium equation was found to be quite fast, attaining an accuracy of 10^{-5} of the ff' values within 3 - 8 iterations depending on the size of the step in the outer iteration loop.

4. Results of Compression Calculations

By applying the computational procedure described above to the general case of a toroidal plasma equilibrium maintained by a constant vertical field, we may determine some characteristics of the behaviour of plasma parameters during major radius compression of an adiabatic plasma. The results presented in Fig. 5 - 8 describe the variations of a number of bulk parameters of the plasma for the case of an initial equilibrium with $\beta_p = 0.67$ which is compressed to 1/3 of the initial major radius at which point the maximum relative error in the q calculation exceeds 10^{-2}. In these results we have calculated the poloidal beta β_p, using the formula

$$\beta_p = \frac{2\bar{p}}{\langle \overline{B_p^2} \rangle_{\psi_c}} = \frac{2 \int p \, dA}{A (\psi_c')^2 K(\psi_c)}$$

, A is the area of the the plasma cross-section

and the toroidal beta β_T, is computed from

$$\beta_T = \frac{2\bar{p}}{\int \frac{B_\phi^2 dV}{V}} = \frac{V \int p dA}{\pi A \int \frac{f^2}{R^2} dA}$$

Flux surfaces corresponding to the initial and final states of this calculation are given in Fig.4.

In comparing these results with the scaling laws determined from the large aspect ratio approximation /5/, we observe that the variations of the volume, average pressure and average minor radius determined from the adiabatic equilibrium calculations are in good agreement with these simple predictions. The behaviour of related parameters such as the average density ($\bar{n} \propto \frac{1}{V}$), temperature ($\bar{T} \propto PV$) and empirically determined scaling for the energy confinement time ($\tau_E \propto \bar{n}\bar{a}^2$) will also conform well with the predicted scalings of $\bar{n} \propto C^2$, $\bar{T} \propto C^{4/3}$ and $\tau_E \propto C$. For the magnetic parameters of the plasma, such as the plasma current, the poloidal beta and, to a lesser ex-

tent, the toroidal beta, howevever, the calculated variations differ considerably from the simple scaling laws. These results demonstrate the effect of including toroidicity, non-circularity of the flux surfaces and finite ß effects in the flux conserving calculation and thus accurately describe the manner in which the plasma energy redistributes itself as a result of the change in external fields.

Calculations of the change in the OH coil flux necessary to prevent skin current formation during compression presented in Fig.8, indicate that, for a total compression ratio of 3, the inductive part of the required OH flux has to be reduced by 18 % under these conditions. If the compression is begun with a higher initial value of $ß_p$, it may be seen from the results given in Fig.8, that the OH flux change required is less, while the total plasma current increases more strongly. We may also observe from the results presented in Fig.7 that, for the higher initial $ß_p$ case, the $ß_p$ falls off more rapidly during compression. This behaviour indicates that the tendency for the plasma to become more paramagnetic as a result of adiabatic compression is larger if the plasma is initially more diamagnetic.

As an indication of the consequences of incorrect programming of the OH system or indeed no control at all, we may estimate the skin current, I_{skin} that would be produced using the relation

$$\Psi_{oh} = L_s \, I_{skin}$$

where L_s is the self-inductance of a toroidal skin current. For a plasma with circular cross-section, this inductance is well approximated by the formula

$$L_s = \mu_o \, R \, (\ell n \, \frac{8R}{a} - 2)$$

where R is the major radius and a the minor radius of the plasma. In the fully compressed state of the calculations described above with R = 0.667 m and a = 0.289 m, we have L_s = 0.768 μH so that a ψ_{OH} value of 0.65 Wb would be produced by a skin current of 847 kA, which corresponds to $\sim$23 % of the total plasma current in the compressed state.

5. Adiabatic Compression in a Compact Ignition Experiment

For the purpose of investigating further details of the plasma behaviour during adiabatic compression as well as the practical feasibility of such a technique, the computational method described above has been used to study the compression phase of the ZEPHYR Compact Ignition Experiment Design /4/. The parameters of the pre-compression plasma are given in Table I together with details of the conductor configurations used for the calculation of the external flux, ψ_{ext} of the vertical field system. Plasma parameter variations during the compression have been investigated for 4 different precompression equilibria with varying β_p. In these calculations, the OH coil system was assumed to have no stray field in the plasma region so that its flux, ψ_{OH} was taken as constant throughout the plasma. Flux surface contours for the initial and final states of the compression phase are given in Fig. 9 for the case with $\beta_p = 1.26$ prior to compression. In all cases studied, the plasma had a mild horizontal elongation before compression (b/a = 0.96 in the case given in Fig.9) and became vertically elongated at the compressed position (b/a = 1.04 for the case with $\beta_p = 1.26$ initially).

The behaviour of the geometric and also averaged kinetic parameters of the plasma (e.g. V, A, $\bar{p}$, $\bar{n}$, $\bar{T}$, τ_E etc.) were again found to be in good agreement with the large aspect ratio scaling predictions while the β_T scaling was typically $\sim$3 % below the predicted $C^{4/3}$ scaling. For each of the initial equilibria considered, the variations of β_p during compression are illustrated in Fig.10. It is possible to explain this behaviour in terms of the rate of increase of the total plasma current (see Fig.11a) which is more rapid than the linear rate predicted by the large aspect ratio theory, resulting in an increased poloidal magnetic field and thus a reduced β_p. When the initial equilibrium has a larger β_p, then the plasma cur-

rent must increase more rapidly to maintain flux conservation during compression and this gives rise to a stronger decrease in β_p.

The magnitude of the vertical field required to compress the plasma increases with β_p as can be seen in the results presented in Fig.11b. Because of this larger contribution of the vertical field, less flux is required to be provided by the OH system to maintain flux conservation if the compression is begun with a higher β_p. This effect can be seen in the calculations of Ψ_{OH} given in Fig.12 where we also observe that the vertical field flux is so large in the highest β_p case, that flux must be subtracted by the poloidal field system. As the β_p decreases during compression, however, the relative contribution of the Ψ_{ext} becomes less so that the Ψ_{OH} required to compensate its effect will be smaller. The behaviour indicated by these calculations demonstrates the desirability of using feedback control of the poloidal field system or at least some form of β_p dependent programming of Ψ_{OH} in order to avoid or limit the occurrence of skin currents during compression.

Profiles of the current density and pressure before and after compression for the case with $\beta_p = 1.55$ initially are shown in Fig.13. These results are illustrative of the behaviour observed in all calculations made using this code, that profiles essentially maintain their initial form during compression so that no strongly localized effects were observed. For the special case of $\beta_p = 1.0$, so that $f(\psi)$ is initially equal to f_o throughout the plasma, it was found that, for the pressure profile corresponding to the initial current density distribution given by eq.(6) with $\alpha_2=0$, the $f(\psi)$ variation produced by compression indicated that the plasma became paramagnetic in the outer regions and diamagnetic closer to the centre (Fig.14). The detection of similar behaviour in the general compression case is complicated by the influence of other stronger effects on the behaviour of the f function, however, in the $\beta_p = 1.0$ region, such variations in the poloidal current distribution due to compression could be important to the stability properties of the plasma.

6. Conclusions

The technique for computing toroidal plasma equilibria conserving adiabatic quantities, which is described in this paper has enabled calculations to be made of the evolution of plasma parameters during major radius compression. In maintaining exact flux conservation in the equilibrium calculations, the variations of the plasma current and the poloidal beta during compression have been found to be substantially different from the scaling predicted by circular, large aspect ratio approximations to the adiabatic behaviour. Geometric and kinetic quantities were, however, found to agree quite well with these simple scaling predictions.

Calculations of the OH coil flux required to prevent the formation of poloidal skin currents during compression have demonstrated the need for considering the influence of the plasma poloidal beta on the operation of the vertical and poloidal field systems. The results indicate the need for a more detailed understanding of the behaviour of a resistive plasma subject to large and relatively fast changes of the external fields which will occur during major radius compression.

Acknowledgements

The authors would like to express their appreciation for the assistance and advice provided by K.Lackner in the performance of this work. They would also like to thank D.B.Nelson for useful discussions concerning the codes developed by himself and H.Grad.

References

/1/ GREEN, R., NOLL, P., SHEFFIELD, J., Plasma Physics 17 (1975), 1101

/2/ ELLIS, R.A., EUBANK, H.P., GOLDSTON, R., SMITH, R.R., NAGASHIMA, T., Nuclear Fusion 16 (1976) 524

/3/ COHN, D.R., JASSBY, D.L., KREISCHER, K., Nuclear Fusion 18 (1978) 1255

/4/ Compact Ignition Experiment, Internal Status Report, September 1978

/5/ FURTH, H.P., YOSHIKAWA, S., Physics of Fluids 13 (1970) 2593

/6/ HOGAN, J.T., Nuclear Fusion 19 (1979) 753

/7/ BOL, K., ELLIS, R.A., EUBANK, H., FURTH, H., JACOBSEN, R., JOHNSON, L., MAZZUCATTO, E., STODIEK, W., TOLNAS, E., Phys. Rev. Lett. 29 (1972) 1495

/8/ GRAD, H., HU, P.N., STEVENS, D.C., Proc.US Nat.Acad. of Science 72 (1975) 3789

/9/ DORY, R.A., PENG, Y-K.M., Nuclear Fusion 17 (1977) 21

/10/ NELSON, D.B., Oak Ridge Nat.Lab.Rep. ORNL/TM-6271 (1978)

/11/ LACKNER, K., Comput Phys.Comm. 12 (1976) 33

/12/ von HAGENOW, K., LACKNER, K., Proc.7th Conf.on Num. Simul.of Plasmas (New York, 1975) 140

/13/ BATEMAN, G., Physics of Fluids 22 (1979) 354

/14/ NELSON, D.B., GRAD, H., Private communication

Table I:

Parameters of ZEPHYR Compact Ignition Experiment Design

Precompression Plasma

Major Radius	2.025 m
Minor Radius	0.61 m
Plasma Current	2.47 MA
Toroidal Magnetic Field	6.1 T
Average Density	$1 - 2 \cdot 10^{20}$ m^{-3}
Safety factor, q	~ 3

Vertical Field Data Design Currents at Full Compression

Coil	Radius(m)	Distance from Symmetry axis(m)	Current(kA)
1	1.6	1.4	558
2	2.4	1.4	930
3	3.4	0.8	1488

Figure Captions

Fig. 1 Geometry of the equilibrium solution.

Fig. 2 Flowchart of the adiabatic equilibrium algorithm

Fig. 3 Convergence of the outer iteration loop for one compression step. The ψ error is the maximum difference between ψ_{tot} values for successive iterations.

Fig. 4 Flux contours before and after major radius compression of a plasma with a uniform vertical field.

Fig. 5 Variations of the total volume V, and average minor radius $\bar{a}$ ($\pi\bar{a}^2$ = cross-section area) with compression ratio $C = \frac{R_o}{R_{pl}}$ where R_{pl} is the major radius of the plasma centre and R_o is the initial value of R_{pl}. Dashed lines indicate the scalings predicted by the simple large-aspect ratio approximation.

Fig. 6 Average pressure $\bar{P}$ and toroidal beta variations during adiabatic compression with $\beta_p = 0.67$ initally.

Fig. 7 Variations of the poloidal beta during compression for high and low initial β_p cases compared with $C^{1/3}$ scaling.

Fig. 8 Behaviour of the total plasma current I_p, and also the flux change of the OH coils, ψ_{OH} during compression. Positive values of ψ_{OH} correspond to a change in the same direction as ψ_{pl}, the plasma flux.

Fig. 9 Flux contours before and after compression for the ZEPHYR Compact Ignition Experiment design values.

Fig. 10 Variations of the poloidal beta with compression ratio, C for initial equilibria with different initial β_p values.

Fig. 11 a) Plasma current variation for compression of plasmas with high and low initial β_p values.

b) Vertical field variation required for compression. The factor B_v is the fraction of the vertical field corresponding to the coil configuration given in Table I which is required for equilibrium.

Fig. 12 OH flux variation required to suppress skin current formation during compression.

Fig. 13 Profiles of the toroidal current density and scalar pressure before and after compression (J in Am^{-2} and P in Nm^{-2}; normalized to μ_o).

Fig. 14 Behaviour of the toroidal field function, f (ψ) during compression for the case with β_p = 1.0 initially.

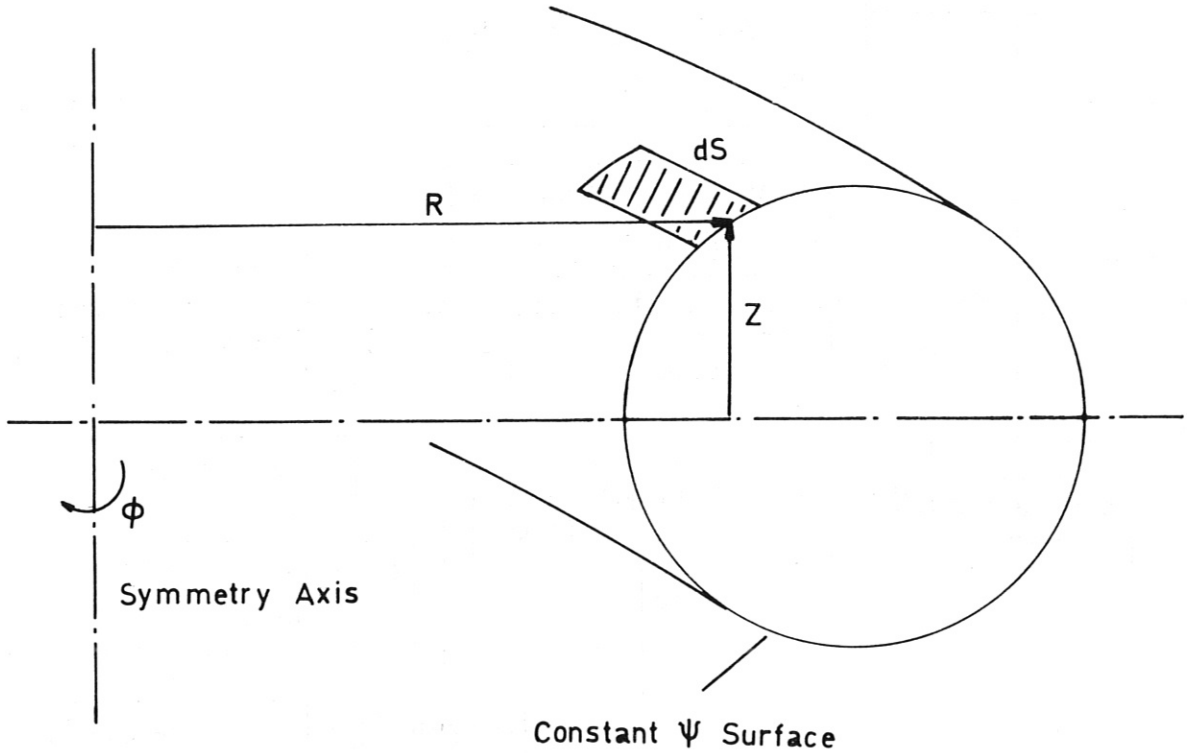

Figure 1

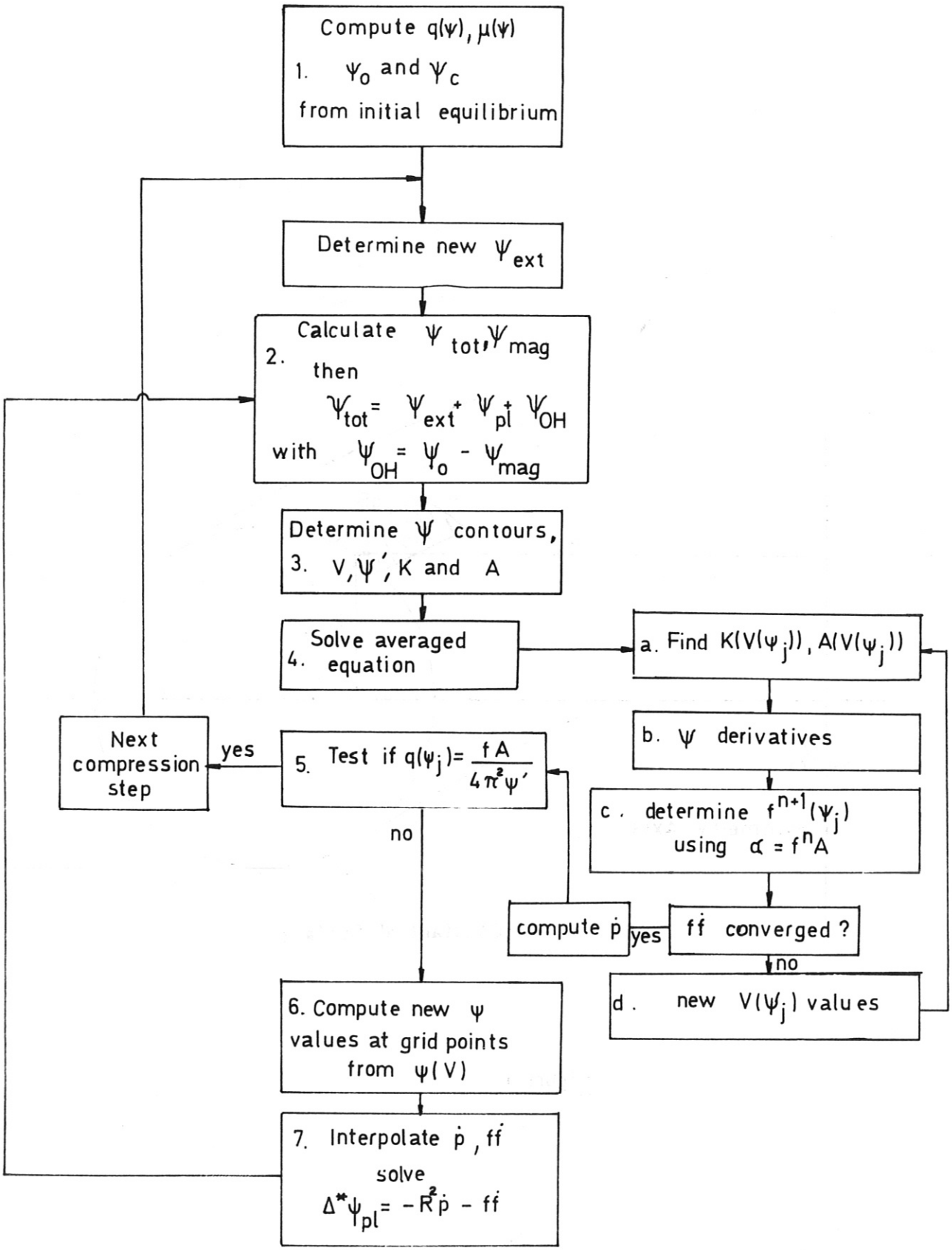
Compute $q(\psi)$, $\mu(\psi)$
1. ψ_0 and ψ_c from initial equilibrium
Determine new ψ_{ext}
Calculate ψ_{tot}, ψ_{mag}
2. then
$\psi_{tot} = \psi_{ext} + \psi_{pl} + \psi_{OH}$
with $\psi_{OH} = \psi_0 - \psi_{mag}$
Determine ψ contours,
3. V, ψ', K and A
Solve averaged
4. equation
a. Find $K(V(\psi_j))$, $A(V(\psi_j))$
b. ψ derivatives
c. determine $f^{n+1}(\psi_j)$ using $\alpha = f^n A$
ff' converged ?
yes
no
compute $\dot{p}$
d. new $V(\psi_j)$ values
5. Test if $q(\psi_j) = \frac{fA}{4\pi^2\psi'}$
yes
Next compression step
no
6. Compute new ψ values at grid points from $\psi(V)$
7. Interpolate $\dot{p}$, ff'
solve
$\Delta^* \psi_{pl} = -R^2\dot{p} - ff'$

Figure 2

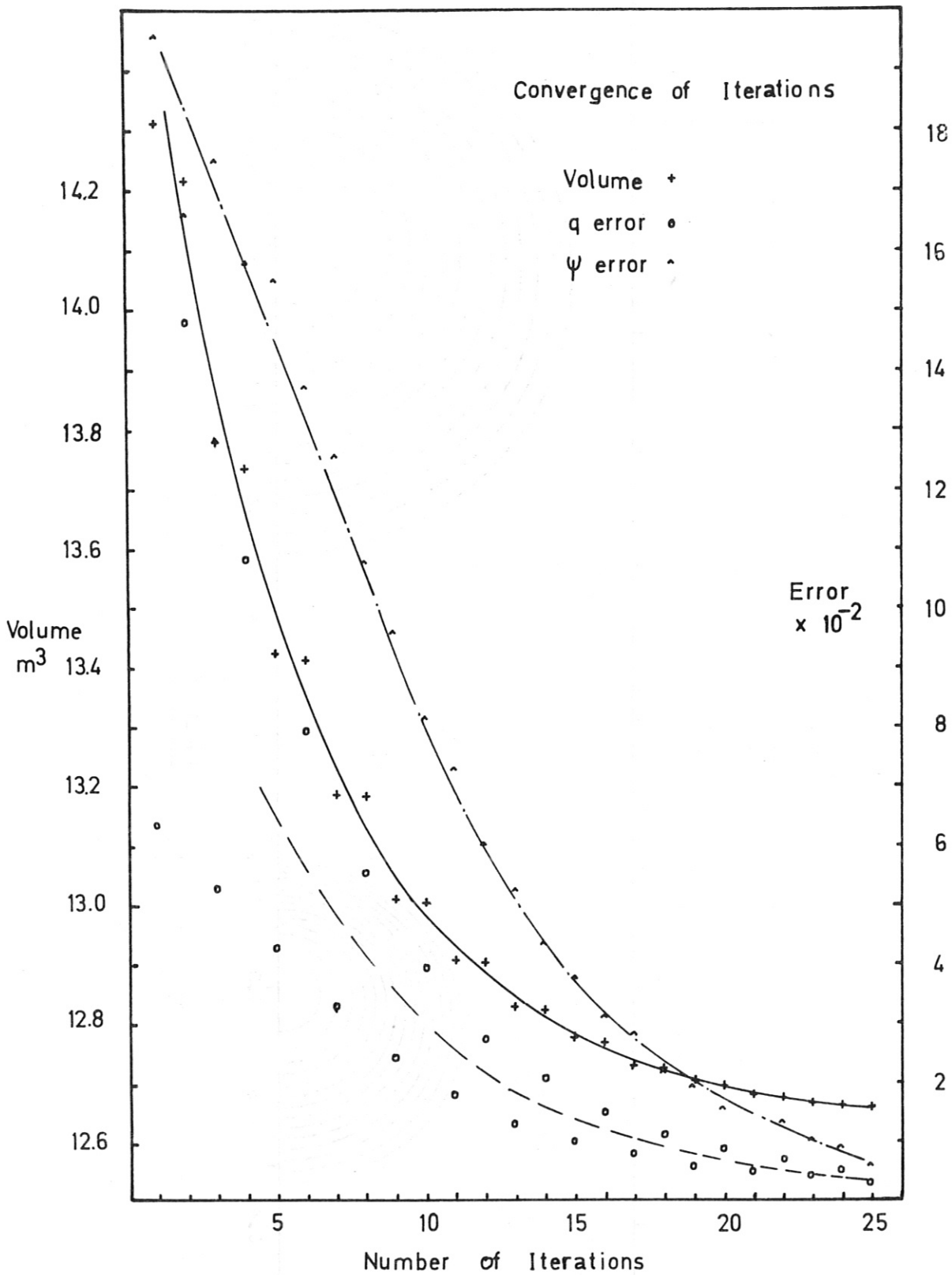
Convergence of Iterations
Volume +
q error o
ψ error ^
Volume m3
Error x 10-2
14.2
14.0
13.8
13.6
13.4
13.2
13.0
12.8
12.6
18
16
14
12
10
8
6
4
2
5
10
15
20
25
Number of Iterations

Figure 3

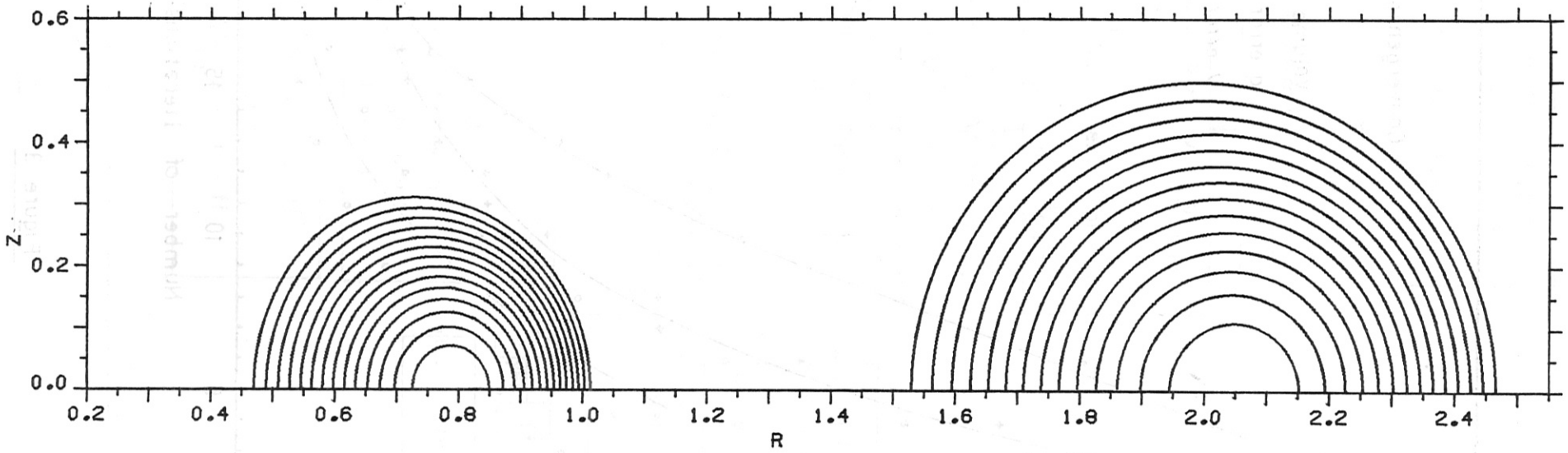

Figure 4

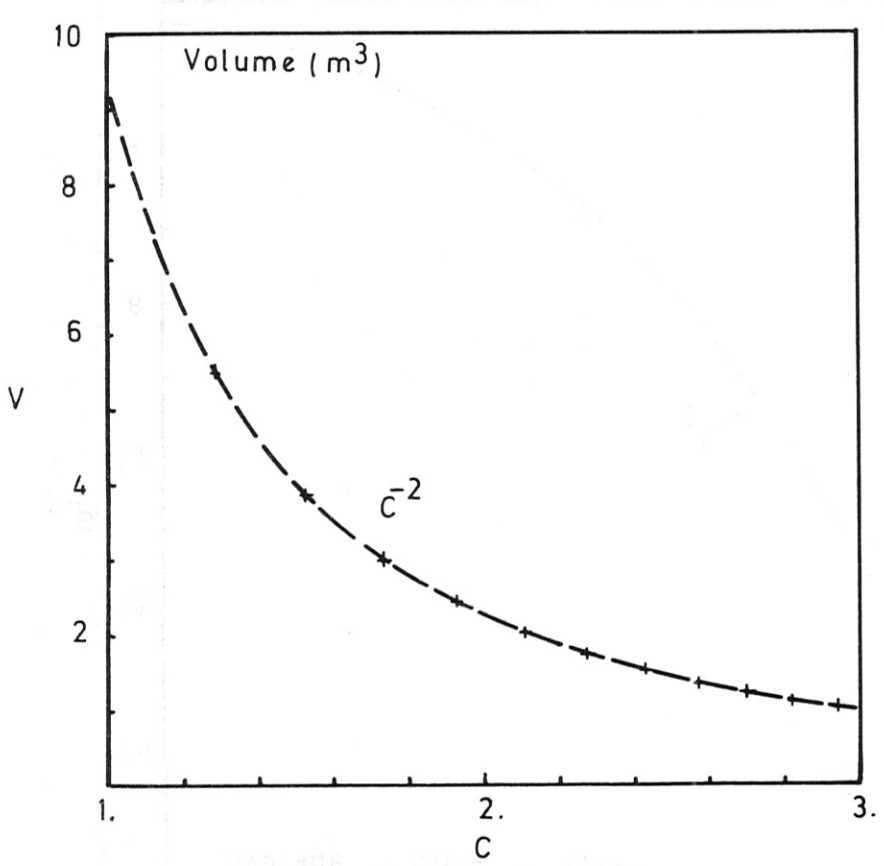

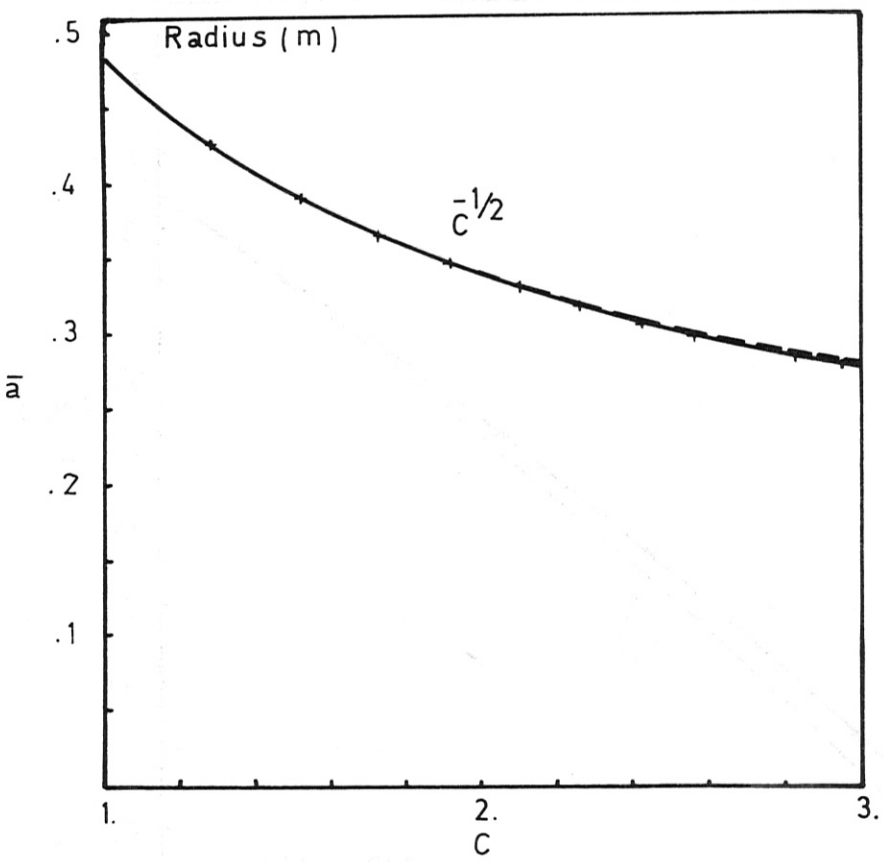

Figure 5

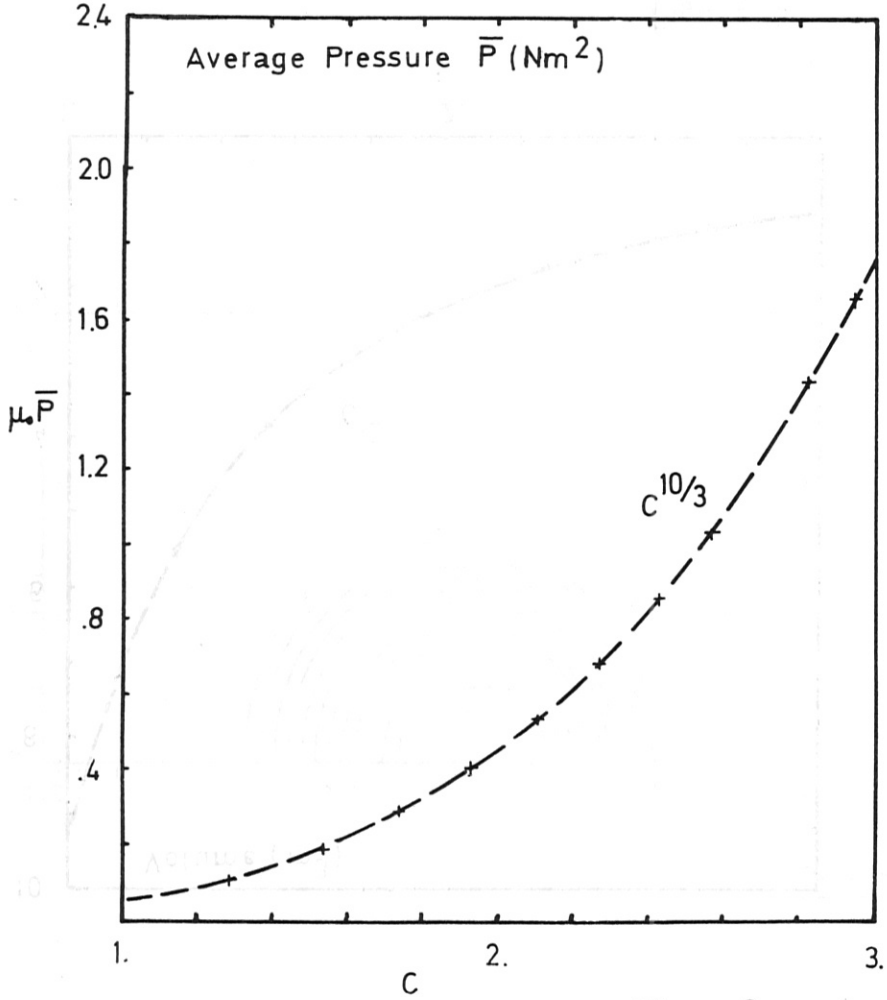
Average Pressure $\overline{P}$ (Nm^2)
$\mu_o \overline{P}$
2.4
2.0
1.6
1.2
.8
.4
1.
2.
3.
C
$C^{10/3}$

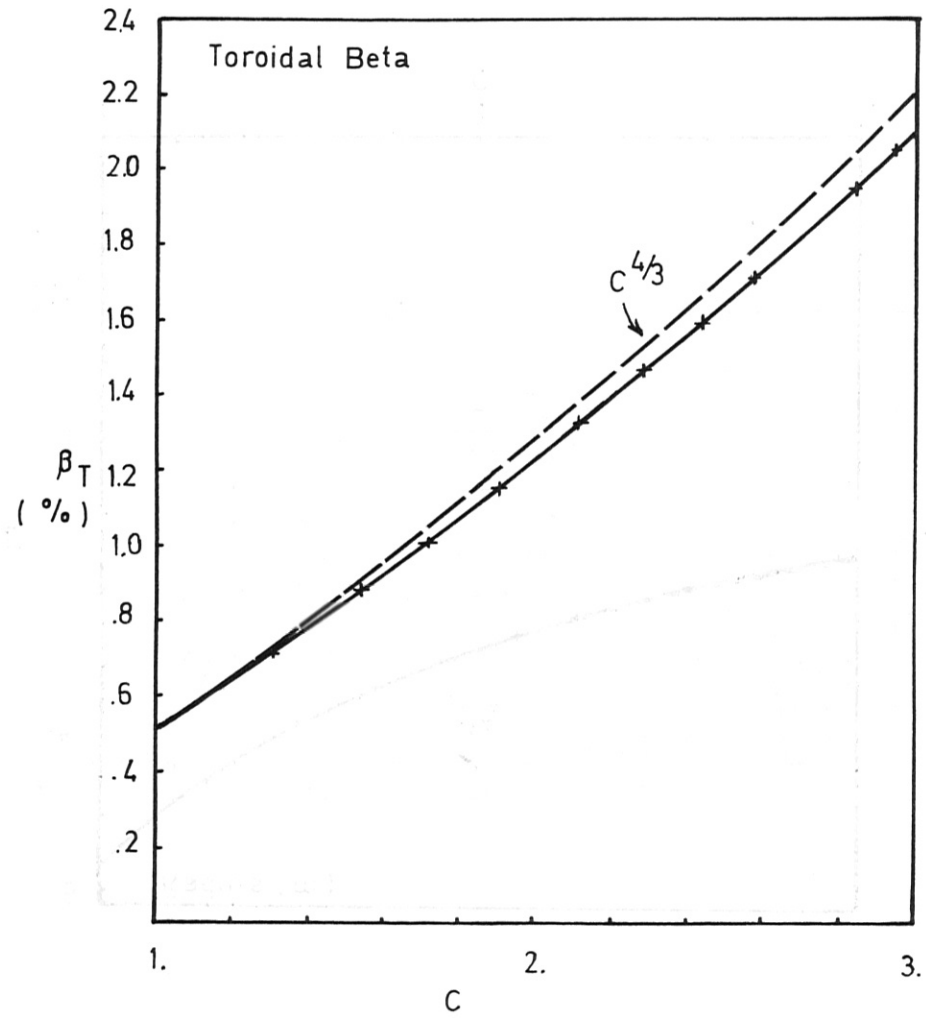
Toroidal Beta
β_T (%)
2.4
2.2
2.0
1.8
1.6
1.4
1.2
1.0
.8
.6
.4
.2
1.
2.
3.
C
$C^{4/3}$

Figure 6

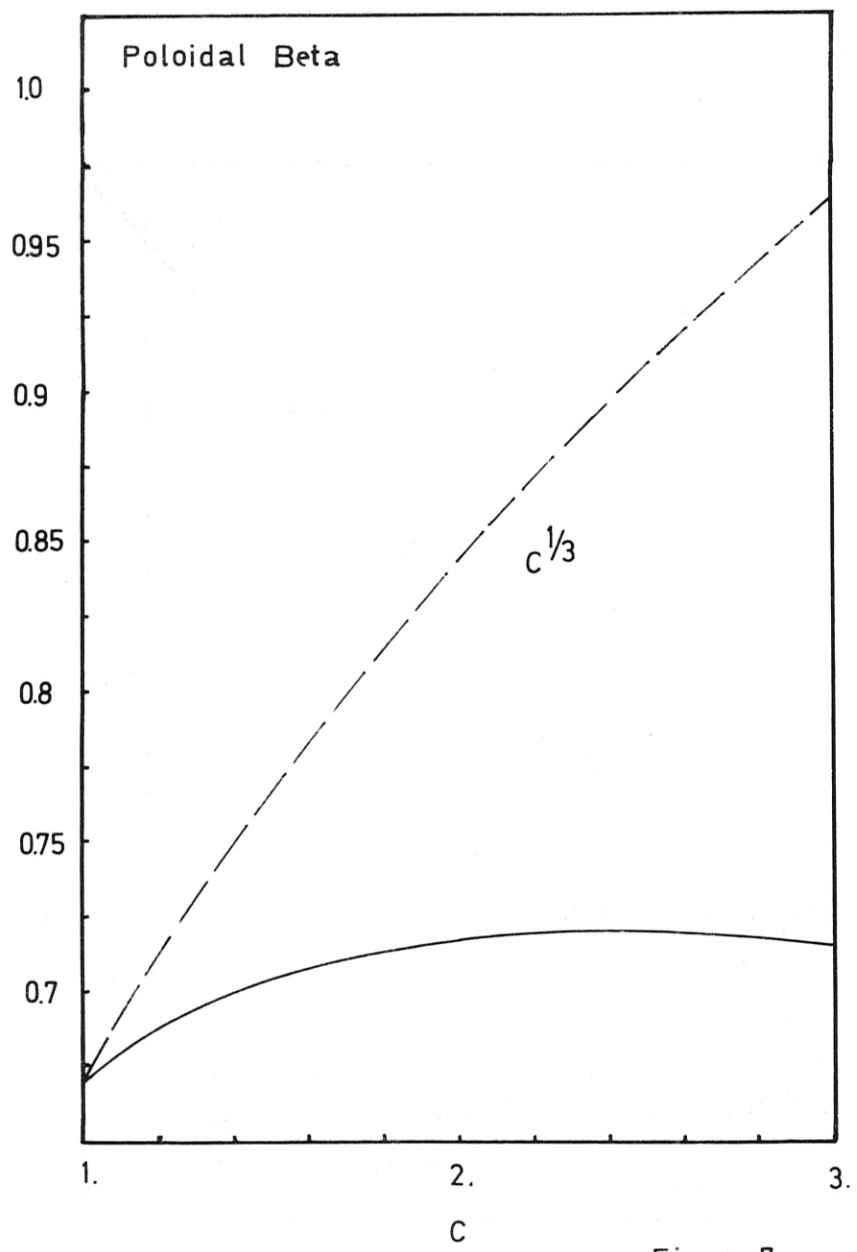
Poloidal Beta
1.0
0.95
0.9
0.85
0.8
0.75
0.7
$C^{1/3}$
1.
2.
3.
C

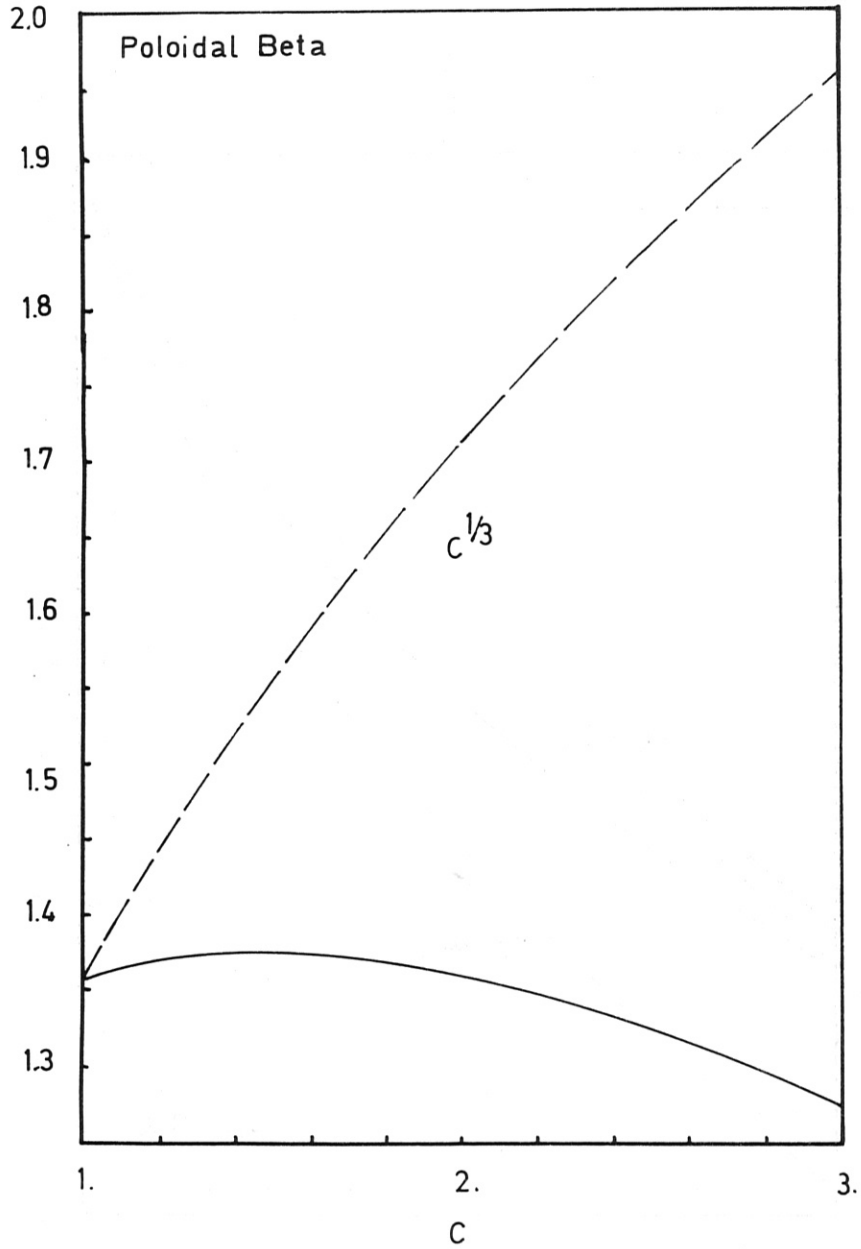
Poloidal Beta
2.0
1.9
1.8
1.7
1.6
1.5
1.4
1.3
$C^{1/3}$
1.
2.
3.
C

Figure 7

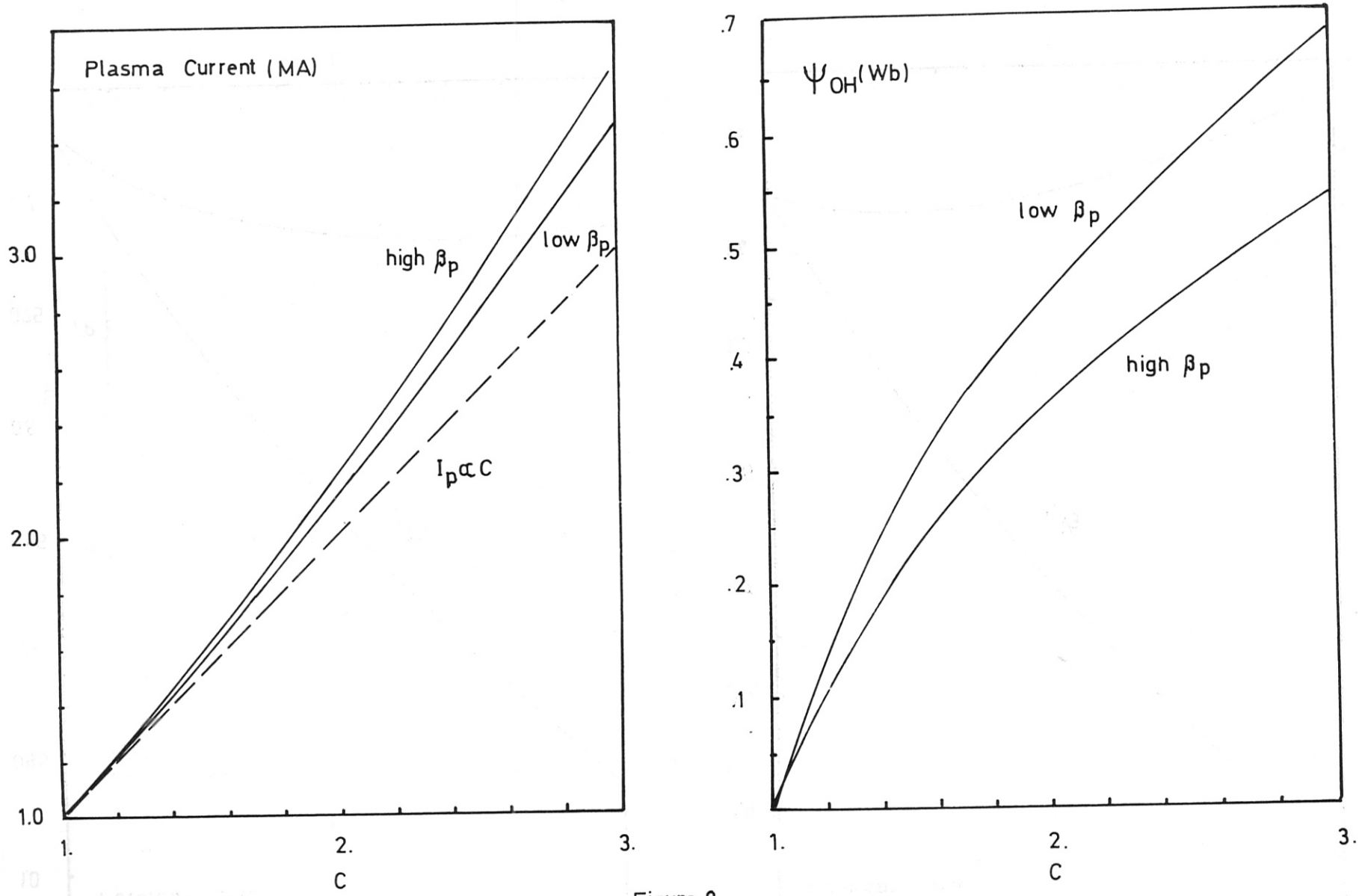
Plasma Current (MA)
3.0
2.0
1.0
high β_p
low β_p
$I_p \propto C$
1.
2.
3.
C
Ψ_{OH}(Wb)
.7
.6
.5
.4
.3
.2
.1
low β_p
high β_p
1.
2.
3.
C

Figure 8

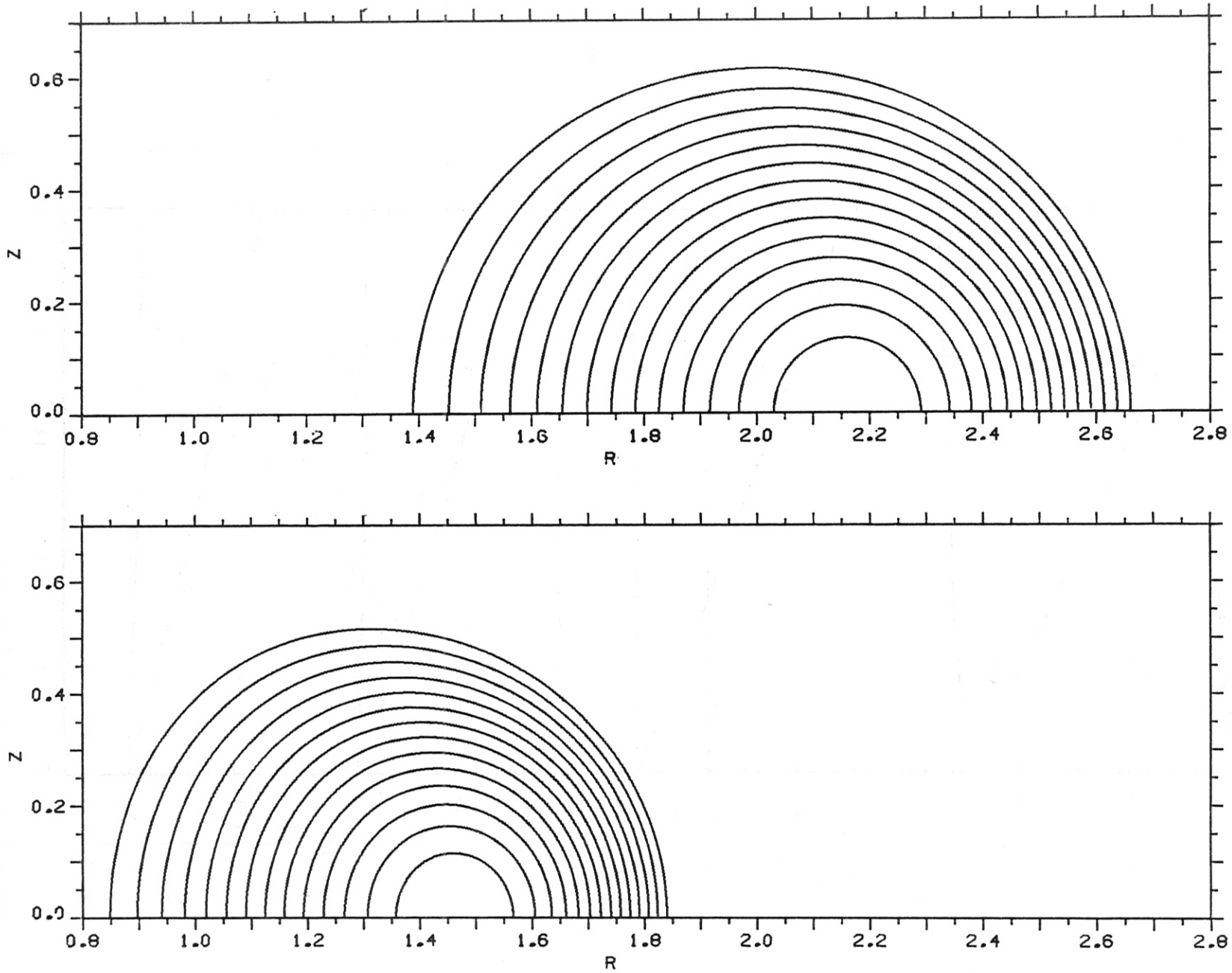
0.6
0.4
0.2
0.0
Z
0.8
1.0
1.2
1.4
1.6
1.8
2.0
2.2
2.4
2.6
2.8
R
0.6
0.4
0.2
0.0
Z
0.8
1.0
1.2
1.4
1.6
1.8
2.0
2.2
2.4
2.6
2.8
R

Figure 9

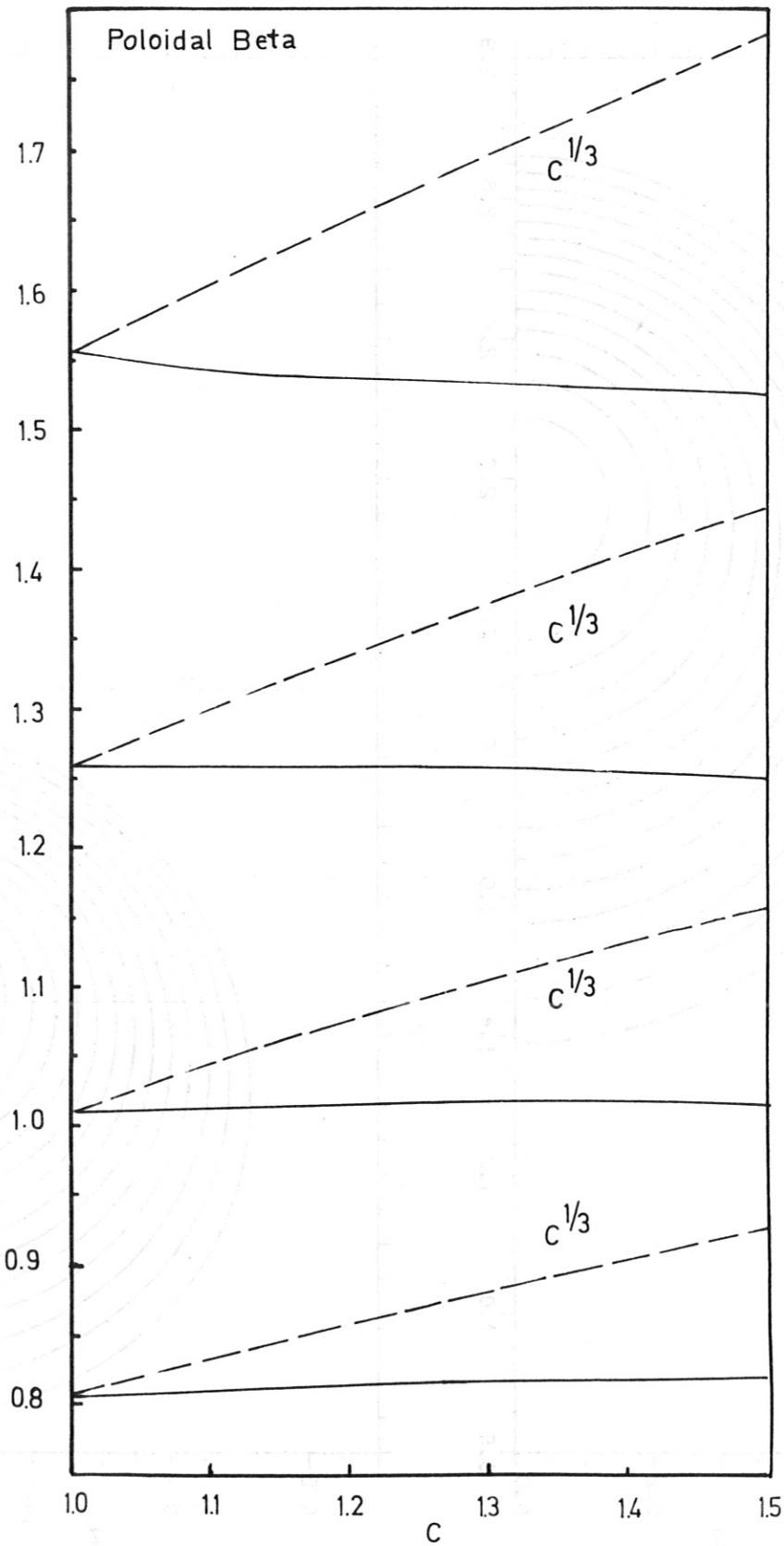
Poloidal Beta
1.7
1.6
1.5
1.4
1.3
1.2
1.1
1.0
0.9
0.8
C 1/3
C 1/3
C 1/3
C 1/3
1.0
1.1
1.2
1.3
1.4
1.5
C

Figure 10

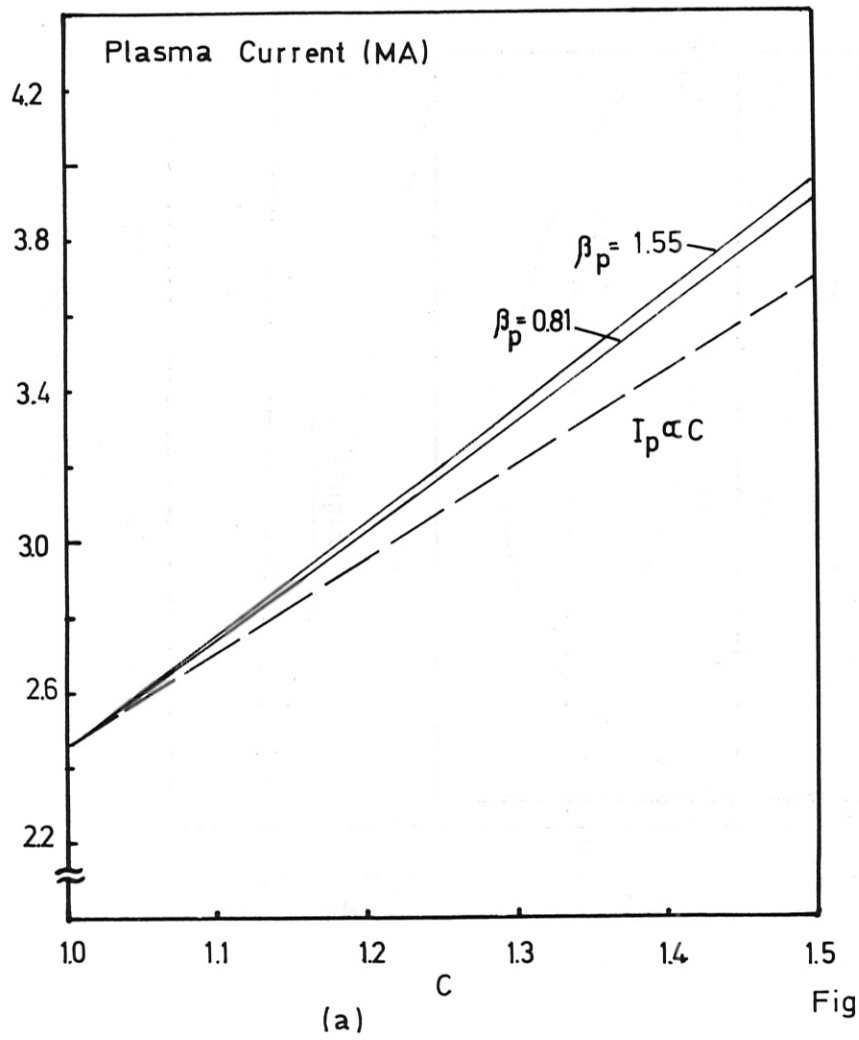
Plasma Current (MA)
4.2
3.8
3.4
3.0
2.6
2.2
β_p= 1.55
β_p= 0.81
$I_p \propto C$
1.0
1.1
1.2
1.3
1.4
1.5
C

(a)

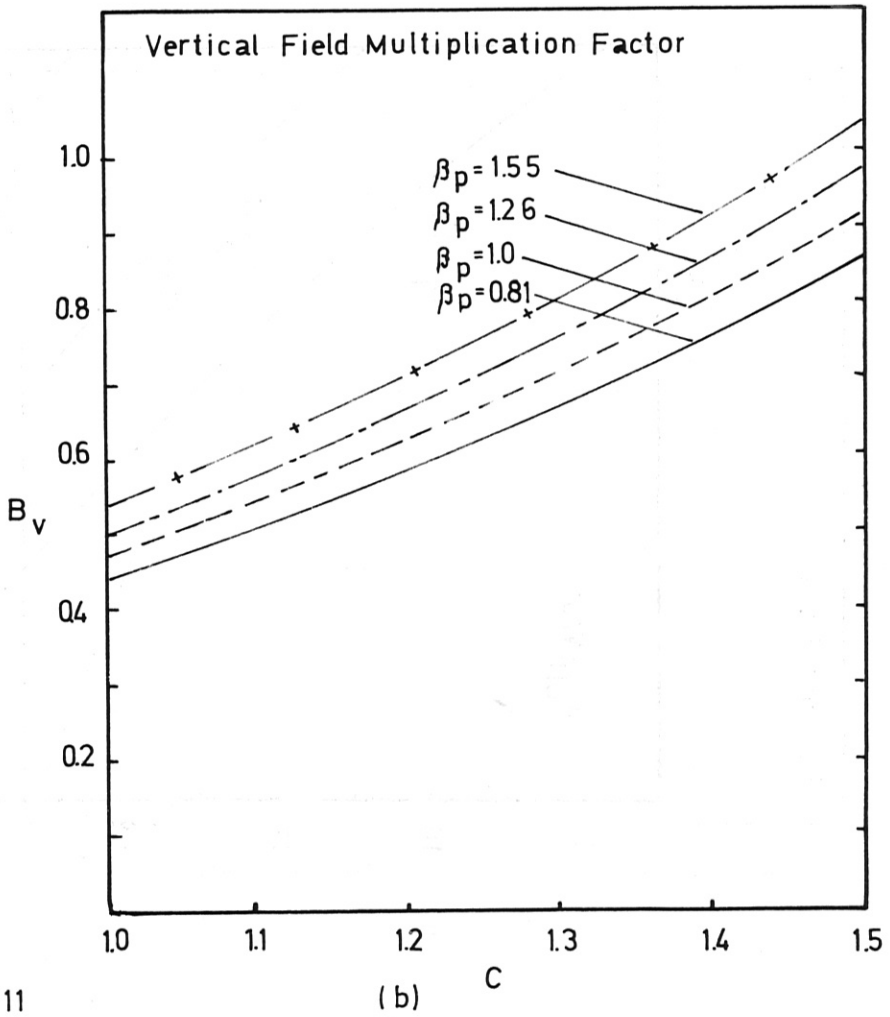
Vertical Field Multiplication Factor
1.0
0.8
0.6
0.4
0.2
B_v
β_p= 1.55
β_p= 1.26
β_p= 1.0
β_p= 0.81
1.0
1.1
1.2
1.3
1.4
1.5
C

(b)

Figure 11

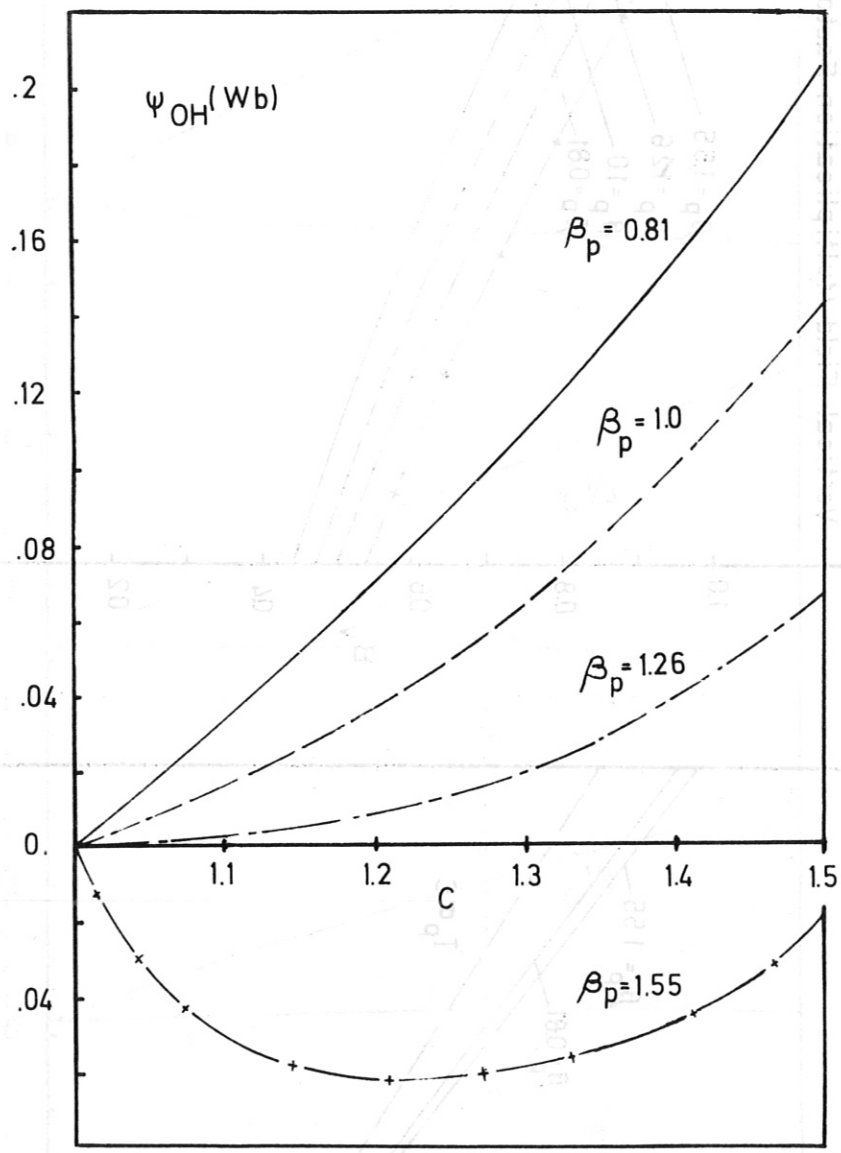
.2
Ψ_{OH}(Wb)
.16
β_p = 0.81
.12
β_p = 1.0
.08
β_p = 1.26
.04
0.
1.1
1.2
1.3
1.4
1.5
C
.04
β_p=1.55

Figure 12

Pre-Compression

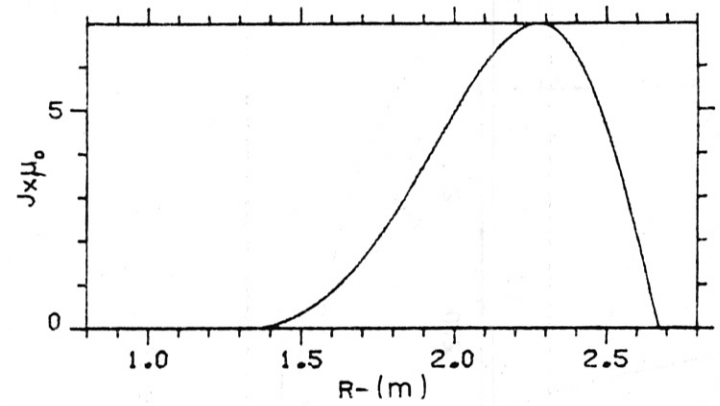

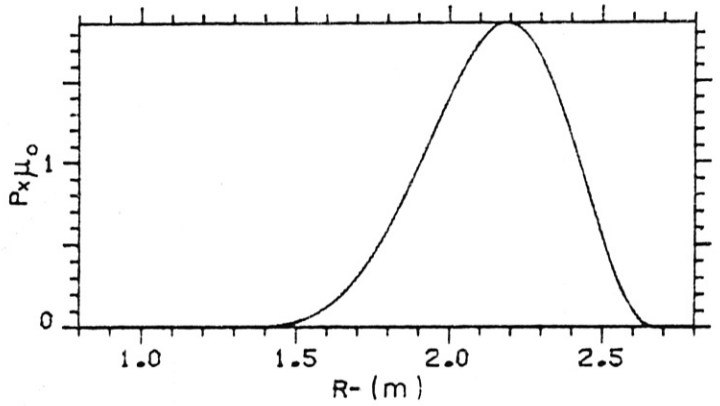

Full Compression

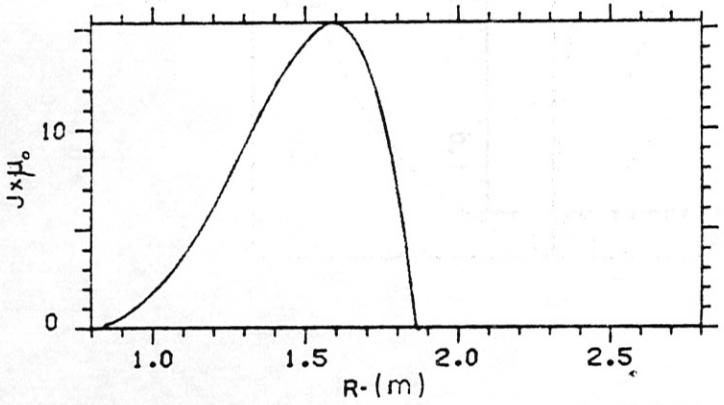

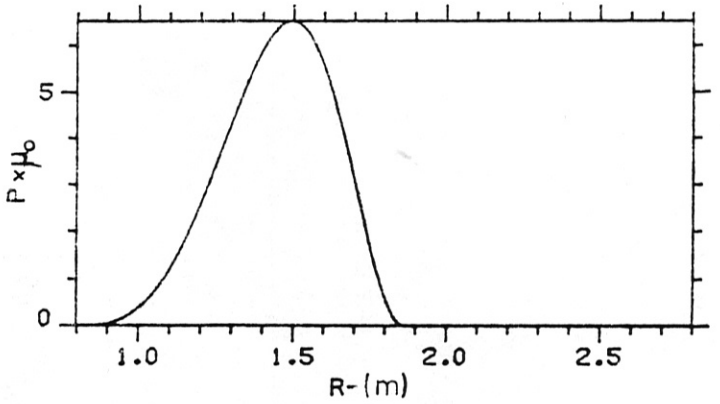

Figure 13

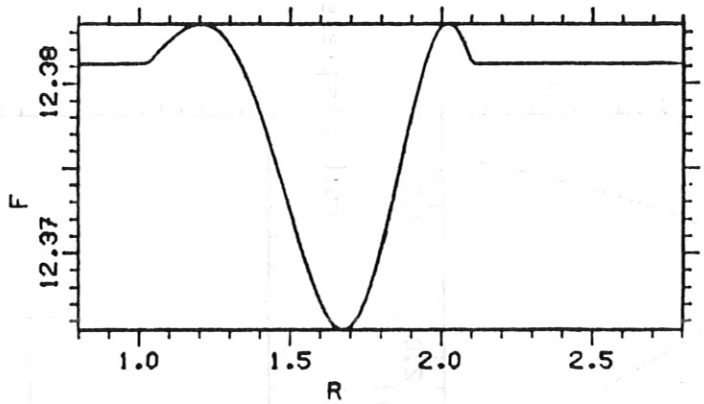

Figure 14